Nanoconfinement effects on the reversibility of hydrogen storage in ammonia borane: A first-principles study

Kiseok Chang,[1] Eunja Kim,[2] Philippe F. Weck,[3] and David Tománek[1,a)]
[1]*Physics and Astronomy Department, Michigan State University, East Lansing, Michigan 48824-2320, USA*
[2]*Department of Physics and Astronomy, University of Nevada Las Vegas, 4505 Maryland Parkway, Las Vegas, Nevada 89154, USA*
[3]*Department of Chemistry, University of Nevada Las Vegas, 4505 Maryland Parkway, Las Vegas, Nevada 89154, USA*

(Received 9 March 2011; accepted 5 May 2011; published online 1 June 2011)

We investigate atomistic mechanisms governing hydrogen release and uptake processes in ammonia borane (AB) within the framework of the density functional theory. In order to determine the most favorable pathways for the thermal inter-conversion between AB and polyaminoborane plus H_2, we calculate potential energy surfaces for the corresponding reactions. We explore the possibility of enclosing AB in narrow carbon nanotubes to limit the formation of undesirable side-products such as the cyclic compound borazine, which hinder subsequent rehydrogenation of the system. We also explore the effects of nanoconfinement on the possible rehydrogenation pathways of AB and suggest the use of photoexcitation as a means to achieve dehydrogenation of AB at low temperatures.
 [doi:10.1063/1.3594115]

I. INTRODUCTION

Hydrogen is widely regarded as a cost-effective, renewable, and clean energy alternative to fossil fuels for transportation applications.[1] From the research effort conducted in solid-state materials capable of storing hydrogen, the NH_3BH_3 compound called ammonia borane (AB), with an ideal storage capacity of 19.5 wt.% H_2 and a reported release,[2,3] of up to ≈13 wt.% H_2 below 200 °C, has emerged as one of the most promising candidate materials to meet the 2015 volumetric ($\gtrsim$82 g H_2 l^{-1}) and gravimetric ($\gtrsim$90 g H_2 kg^{-1}) density targets specified by the U.S. Department of Energy for on-board hydrogen storage.[4]

At room temperature, AB crystallizes in a stable plastic phase with the tetragonal *I4mm* structure.[5] Upon thermally induced decomposition, AB releases H_2 in a two-step exothermic process.[2,3,6–8] The initial dehydropolymerization step occurs between 343 K and 385 K, yielding ≈1 mol H_2 and polyaminoborane (PAB) products, $[BH_2NH_2]_n$ ($\Delta H = -1.57$kcal mol^{-1}).[9] PAB further decomposes in the temperature range of 383 − 473 K, releasing hydrogen and polyiminoborane (PIB) products, $[BHNH]_n$ ($\Delta H \approx -9.5$kcal mol^{-1}).[9] The ultimate decomposition step leading to the formation of planar BN at ≈1500 K is not considered practical for storage purposes. Several species, such as borazine (c-$B_3N_3H_6$), cycloborazanes, or diammoniate of diborane (DADB, $NH_3BH_2NH_3$+BH_4), have been observed concurrently to the formation of PAB and PIB, depending on the decomposition conditions of AB.[3,6–8,10,11]

Some mechanistic and thermodynamical aspects of these decomposition processes have been investigated in recent computational studies.[9,12–15] Still, the microscopic pathway of the AB dehydrogenation process has not been understood in full detail yet. Also, optimum conditions have yet to be found for AB rehydrogenation and suppression of volatile by-products such as borazine, which can poison the catalyst material of proton exchange membrane fuel cells. Recent approaches to remedy these problems have focused on tuning thermodynamic properties and controlling reaction pathways using catalysts,[15–17] modified AB materials,[18,19] ionic liquid solvents,[10] or encapsulating AB in mesoporous materials.[20–23] Even though significant experimental advances have been achieved, fundamental understanding of these processes is still missing.

In this manuscript, we study the governing mechanisms associated with hydrogenation and dehydrogenation processes of ammonia borane. Our objective is to better utilize this unique material by examining the energy profiles associated with the conversion of the AB molecular solid to polymeric molecules and hydrogen. We first investigate the two-step dehydrogenation process and then explore encapsulation of AB molecules inside nanopores and nanotubes as a potentially viable pathway for AB rehydrogenation.

Details of our computational approach are given in Sec. II, followed by a discussion of our results in Sec. III. A summary of our findings and conclusions is given in Sec. IV.

II. COMPUTATIONAL METHOD

First-principles total-energy calculations based on density functional theory (DFT) were carried out using the SIESTA code[24] to determine the optimum geometry of AB in the solid phase and to examine energetically preferred pathways for the dehydrogenation and rehydrogenation processes. We used the standard Kohn-Sham self-consistent method within the local density approximation with the Perdew-Zunger[25] parametrization of the

a)Electronic mail: tomanek@pa.msu.edu.

exchange-correlation functional in the uniform electron gas. Since the weak inter-molecular interactions in our system are dominated by electrostatic and weak covalent interactions causing band dispersion, this energy functional should provide an adequate description of the equilibrium structure and elastic properties.[26] We furthermore used a general and flexible linear combination of numerical atomic orbital basis and norm-conserving Troullier-Martins pseudopotentials[27] in the nonlocal Kleinman-Bylander form.[28] Our basis consisted of pseudo-atomic-orbitals (PAOs) generated by the split-valence scheme for a double-ζ polarization basis set. All calculations were performed using periodic boundary conditions in supercell geometry. Depending on the context of a particular calculation, we used supercells containing two or more AB molecules. We sampled the reciprocal space by $k-$point grids with comparable densities in all our calculations, with the minimum number of $6k$ points in the smallest Brillouin zone. We limited the energy shift due to the spatial confinement of the PAO basis functions[29,30] to less than 30 meV. The charge density and pseudopotentials have been determined on a real space grid with a very high mesh cutoff energy of 200 Ry, which is sufficient to converge the total energy to within 1 meV/atom. We used the conjugate gradient method for geometry optimization. A structure was considered optimized when none of the residual forces exceeded 0.01 eV/Å. Complementary microcanonical molecular dynamics (MD) simulations were performed at the same level of theory to investigate the thermodynamical properties and the microscopic pathways for the dehydrogenation processes. A time-step of 1 fs was used in all simulations with a maximum simulation time of 2 ps. The temperature range of our MD simulations extended up to 1500 K.

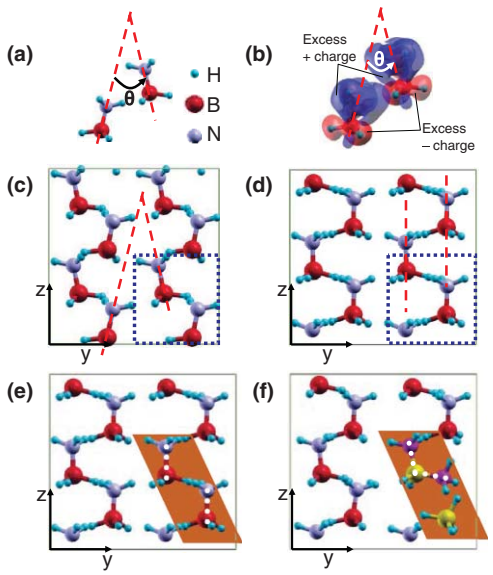

FIG. 1. Optimized geometry of orthorhombic and tetragonal crystals of AB and DADB-AB. (a) Local geometry of AB molecules, with θ denoting the angle between neighboring molecules in the orthorhombic crystal. (b) Charge difference plot depicting two AB molecules. Larger lobes, highlighted in blue, indicate the region with excess positive charge and smaller lobes, highlighted in red, the region with excess negative charge, establishing a permanent dipole. The dipole-dipole interaction stabilizes the dihydrogen-bond network moment in the crystal. (c) Optimized structure of the orthorhombic crystal with $\theta = 22^\circ$ ($\theta_{\text{expt}} = 20.4^\circ$). (d) Optimized structure of the tetragonal crystal with all AB molecules aligned along the same direction. Optimized structure of two AB molecules (e) and DADB (f) in the AB tetragonal crystal. The region, where the 2AB→DADB transformation takes place, is shaded in (e) and (f). The backbones of AB and DADB involved in this reaction are highlighted by the white dotted lines in (e) and (f). B and N atoms in DADB are distinguished by shading in (f).

III. RESULTS AND DISCUSSION

We have studied the structure and energetics of AB and related compounds in order to find the most efficient microscopic reaction pathways for the dehydrogenation and rehydrogenation processes and investigated new possible methods for efficient rehydrogenation of AB under mild conditions. We have focused our studies on identifying the different crystal structures of AB, the equilibrium structure of DADB and its formation energetics, and the microscopic pathway of AB dehydrogenation processes. We have then explored possible ways to improve the de- and rehydrogenation process of AB by using photoexcitations and by confining BN-based molecules in narrow carbon nanotubes (CNTs).

A. Crystal structures of AB and the role of the dihydrogen bond

Boraneamines in the condensed phase show a propensity to form $\text{N}-\text{H}^{\delta+}\cdots^{\delta-}\text{H}-\text{B}$ close contacts as a result of the inter-molecular interaction between the NH proton and the adjacent HB bond, as seen in Fig. 1(a). For this peculiar type of hydrogen bond, commonly referred to as the dihydrogen bond, the $\text{H}\cdots\text{H}$ distance is typically in the range of $1.7 - 2.2$ Å, thus significantly shorter than the sum of the van der Waals radii of two hydrogen atoms, 2.4 Å. The hydrogen atom connected to nitrogen carries a partial positive charge ($\text{H}^{\delta+}$) and the hydrogen atom connected to boron a partial negative charge ($\text{H}^{\delta-}$), as seen in Fig. 1(b). Along with the covalent $\text{N}-\text{H}\cdots\sigma$ bonds, the weaker $\text{N}-\text{H}^{\delta+}\cdots^{\delta-}\text{H}-\text{B}$ dihydrogen interactions with a bond strength of ≈0.3 eV, stabilized by the Coulomb attraction between hydrogen atoms carrying opposite charges, largely contribute to stabilizing the molecular crystal at room temperature. At this point, it is useful to remember that ethane, the homonuclear equivalent to AB with no dihydrogen bonds, is not a solid, but rather forms a gas at room temperature.

Our calculations show that the lowest-energy crystal structures of AB are orthorhombic and tetragonal molecular crystals, depicted in Figs. 1(c) and 1(d). According to experiment, the low-temperature orthorhombic structure of AB undergoes a phase transition to the high-temperature tetragonal phase[31–33] at 225 K. The optimized structure of the $Pnm2_1$ orthorhombic lattice is characterized by the lattice constants $a = 5.142$ Å, $b = 4.588$ Å, $c = 4.772$ Å, and the angle $\theta = 20^\circ$ between neighboring AB molecules. This structure, shown in Fig. 1(a), agrees rather well with experimental data.[32,34] The small difference between the finite-temperature experimental value $\theta_{\text{expt}} = 20.4^\circ$ and the theoretical value $\theta_{\text{theo}} = 22^\circ$ obtained at $T = 0$ may be attributed to anharmonicities in the interactions that are explored in the molecular crystal at nonzero temperatures.

At $T = 0$, we find the orthorhombic $Pnm2_1$ crystal to be energetically more stable than the tetragonal $I4mm$ crystal by 49 meV per AB molecule. At higher temperatures, changes in the vibrational entropy difference between the phases may overcome this small energy difference, causing a phase transition. We find support for this general finding in our MD calculations, which indicate a stability reversal between the tetragonal and orthorhombic phase in terms of free energy differences between 200 and 300 K, which is very close to the experimental value of 225 K.

B. Energetics and structural changes during the DADB formation

Formation of diammoniate of diborane within the AB crystal is governed by changes in the dihydrogen bond network, which we study in a suitable supercell geometry. According to our calculations, the DADB molecule possesses a large dipole moment comparable to that of the AB molecule. Also, the potential energy of DADB in the AB crystal is comparable to that of AB in crystalline phase. To study the coexistence of DADB with AB, we substituted DADB for two AB molecules in the tetragonal molecular crystal, as shown in the brown shaded region of Fig. 1(e) (optimized AB crystal geometry) and Fig. 1(f) (optimized DADB geometry in the AB crystal). The large dipole moment of DADB further stabilizes the dihydrogen bond network, since the potential energy of the DADB tetragonal crystal is lower than that of the perfect AB tetragonal crystal by 34 meV per AB molecule.

In terms of potential energy at $T = 0$, the perfect defect-free orthorhombic AB crystal is the most stable structure, followed by the DADB tetragonal crystal, and finally the perfect defect-free AB tetragonal crystal as the least stable of the three. Considering the fact that the tetragonal and orthorhombic AB crystal structures coexist at room temperature, formation of DADB in AB crystals is to be expected on energy grounds, with supporting experimental evidence.[33] The geometry of $NH_3BH_2NH_3$ in DADB is similar to that of polyaminoborane, the product of the first stage of dehydrogenation.

C. Microscopic pathway of the dehydrogenation process

Inspection of our microcanonical molecular dynamics simulations at an average effective temperature of ≈1500 K reveals that hydrogen atoms attached to nitrogen and boron in ammonia borane are released and associate to a hydrogen molecule for a 20 fs time period. This process can be understood by studying reactions involving chains of AB molecules with one AB molecule per unit cell, as seen in the inset of Fig. 2(a). In this particular study, we artificially increased the inter-chain separation to suppress the influence of neighboring AB chains. To get detailed understanding of the optimum transition path independent of temperature and particular trajectories used in MD runs, we explore the potential energy surface of the system by performing constrained geometry optimizations and show the results in Fig. 2(a). In the first dehydrogenation scenario $NH_3BH_3 \rightarrow NH_2BH_2 + H_2$, we consider pairs of distances (d_{N-H}, d_{B-H}) within the unit cell as indicated in the inset of Fig. 2(a). Since the dehydrogenation process occurring in nature can be characterized by a sequence of (d_{N-H}, d_{B-H}) distance pairs, we use it as a prejudice-free reaction coordinate to characterize the reaction pathway. The potential energy surface $E(d_{N-H}, d_{B-H})$, presented in Fig. 2(a), is the result of few hundred structure optimization studies, each of which considered specific values for the d_{N-H}, d_{B-H} distances that were kept fixed along with the unit cell size. The optimum trajectory from the initial geometry M_1, representing the equilibrium structure of AB in the crystal, over the barrier B to the final state M_2 containing an H_2 molecule per unit cell, is shown by the dashed line in Fig. 2(a). The corresponding energy profile and structural snap shots along this trajectory, which corresponds to the reaction coordinate, is depicted in Fig. 2(c). The reaction $NH_3BH_3 \rightarrow NH_2BH_2 + H_2$ requires crossing the activation barrier of 1.14 eV per AB molecule. The net process is endothermic, requiring a 0.75 eV energy investment to occur, which is the reason for the short 20 fs time period during which a hydrogen molecule was formed as a result of temperature fluctuations in our microcanonical MD simulation.

Since dehydrogenation occurs as an activated exothermic process in nature, the final product should be more stable than isolated NH_2BH_2 molecules. A possible final product of the dehydrogenation of AB, which satisfies this condition, is polyaminoborane $[BH_2NH_2]_n$. The second scenario of the dehydrogenation reaction that involves AB polymerization, $nNH_3BH_3 \rightarrow [NH_2BH_2]_n + nH_2$, is described in Figs. 2(b) and 2(d) and is indeed mildly exothermic. In analogy to the first dehydrogenation scenario, we considered pairs of distances (d_x, A_z), shown in the inset of Fig. 2(b), useful to identify a prejudice-free reaction coordinate with focus on the polymerization. Also in this case, we artificially increased the size of the unit cell normal to the z axis to suppress the influence of AB molecules away from the z-axis. The potential energy surface $E(d_x, A_z)$, presented in Fig. 2(b), is the result of few hundred structure optimization studies, each of which considered specific values for d_x and A_z. In our calculation, we consider two AB molecules per unit cell and keep their axes along the BN bond parallel to each other separated by d_x. We expect the AB polymerization process to be initiated by reducing d_x, accompanied by changes in the unit cell size A_z in the axial direction. The most efficient pathway for this process, depicted by the white dashed line in Fig. 2(b), indeed follows our expectations. Separation of the H_2 molecule from $[NH_2BH_2]_n$ is a necessary side-effect in the final state of the polymerization. Even though the net process is exothermic, it involves rather high activation barriers, as seen in Fig. 2(d). The activation barrier values of 4.29 eV and 3.35 eV in the second scenario are much larger than the value of 2×1.14 eV in the first scenario with two AB molecules per unit cell. The origin of these high activation energy values is the strong inter-molecular repulsion and the reduced stability of the NH_2BH_3+H and NH_3BH_2+H complexes associated with the transition states. Even though these high activation energy values are expected to decrease, when artificial constraints such as relative axis orientation are relaxed, this reaction is unlikely to occur under experimental conditions.

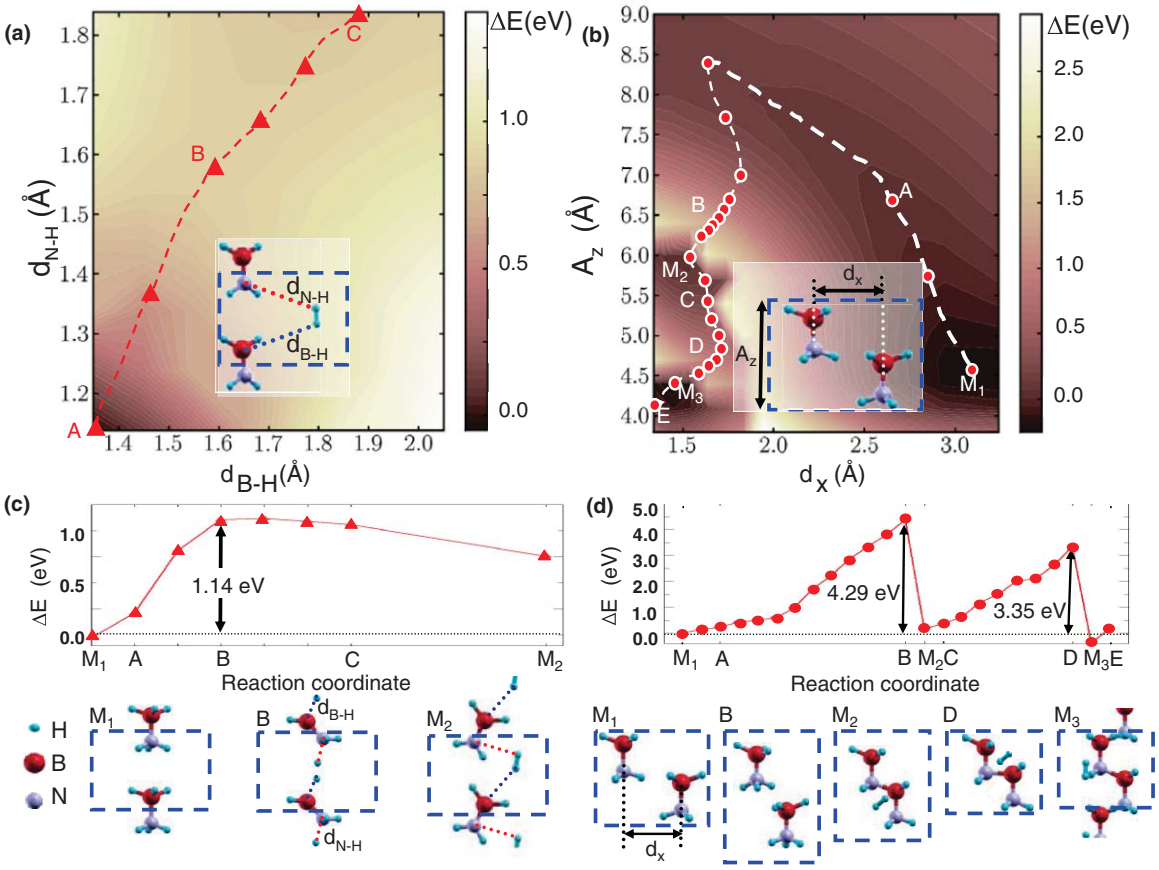

FIG. 2. Microscopic pathways of the dehydrogenation process. (a) Contour plot of the potential energy surface as a function of d_{B-H} and d_{N-H} in the first dehydrogenation scenario, $NH_3BH_3 \rightarrow NH_2BH_2 + H_2$, with d_{B-H} and d_{N-H} defined in the inset. The optimum dehydrogenation pathway is indicated by the dashed line. (b) Contour plot of the potential energy surface as a function of d_x and A_z in the second dehydrogenation scenario, $nNH_3BH_3 \rightarrow [NH_2BH_2]_n + nH_2$. (c) Potential energy profile along the reaction coordinate for the first scenario. The selected structures (M_1, B, M_2), are the snapshots in the process. M_1 and M_2 are the globally relaxed geometries of A and C, respectively. B is the saddle point geometry on the potential energy surface. The dashed rectangle is the unit cell used in the calculation. (d) Potential energy profile along the reaction coordinate for the second scenario. Local minimum (M_1, M_2, M_3) and intermediate structures (B, D) are shown below.

Another possible scenario of dehydrogenation involves intermediate structures such as $NH_3BH_2NH_3$+BH_4 (DADB) in the process. The formation of DADB in the dihydrogen bond network is energetically favorable due to its high polarity. Moreover, from a structural viewpoint, DADB is reminiscent of a polymer. To check on the viability of this process, we calculate the potential energy surface of the DADB formation. In our model calculation we consider the formation of DADB from two isolated AB molecules. We find that a likely reaction may start with an initial dissociation of one of the AB molecules into NH_3 and BH_3. Association of the ammonia and AB molecules would lead to the formation of $NH_3BH_2NH_3$, accompanied by the release of hydrogen from the BH_2 site. Even though this reaction is weakly exothermic, in agreement with experimental observations,[2] the activation barrier of 3.59 eV for this process appears too high, possibly due to the low stability of intermediate structures in our isolated system. Thus, we conclude that this reaction is unlikely to take place.

In view of the fact that the observed thermolysis of AB is weakly exothermic and occurs under mild conditions,[2] we must conclude that this process is likely much more complex than described here. We can only speculate about more favorable ways to form DADB in the AB molecular crystal, including autocatalytic reactions assisted by diffusing hydrogen atoms in the matrix, since presence of hydrogen may reduce the activation barrier for the formation of DADB. Once $NH_3BH_2NH_3$ forms in the crystal, its presence can promote exothermic polymerization of AB by dehydrogenation. It is fair to assume that at any given point, we may find PAB segments of different length and possibly even branched polymers among the dehydrogenation products. We observe nonvanishing net charges only at the extremities of these products. Since the dihydrogen bonds, which are responsible for the formation of the molecular crystal, are stabilized by Coulomb attraction between charged extremities, the mixture of different dehydrogenated polymers will likely form a disordered dihydrogen-bonded network that bears little resemblance with the ordered AB crystal.

D. Photo-assisted dehydrogenation

Achieving dehydrogenation under mild conditions is another challenge if AB is to become a practical hydrogen storage medium. Most research effort in this area has focused on the use of chemical catalysts to reduce the activation barrier for dehydrogenation in order to lower the reaction

temperature. Here, we explore an alternative way to accelerate dehydrogenation by modifying the interatomic interactions in the photo-excited state. To study deviations from dynamics in the ground state with electrons at $T_{el} = 0$, we repopulate the electronic levels according to the Fermi-Dirac distribution at $T_{el} > 0$, which modifies the charge distribution and thus the potential energy surface. Using $k_B T_{el} = 2$eV for the effective electronic temperature, which may be achieved by laser irradiation,[35] we find that the activation barrier for $NH_3BH_3 \rightarrow NH_2BH_2 + H_2$ is 0.61 eV per AB molecule, which corresponds to nearly a 50% reduction from the previously stated ground-state value 1.14 eV. This result indicates that changes in the potential energy surface associated with electronic excitations can be significant. This reduction of the activation barrier is partly caused by changing the population of molecular orbitals that modifies the force field. Additional contributions to the free energy come from electronic entropy and also depend on geometry. In the present case, the electronic entropy contribution at the global minimum geometry is $S_e = 6.16k_B$, whereas the contribution at the saddle point corresponding to the transition state is $S_e = 6.60k_B$. At nonzero temperatures, this effect reduces the free energy activation barrier and thus speeds up the reaction.

E. Energetics of B–N based molecules inside a carbon nanotube

Even though AB is one of the best candidates for hydrogen storage, it is not clear how to rehydrogenate products of the decomposition reaction in an efficient and cost-effective way. Here we explore the possibility to utilize narrow CNTs as a generic AB storage medium that may facilitate the rehydrogenation process, ignoring for the moment the fact that adding nanotubes would increase the weight and thus reduce the storage capacity. The objective is to form ordered AB arrays within the narrow space inside the CNTs in order to control the polymerization pathway during dehydrogenation and thus to facilitate rehydrogenation.

We investigated the energetics of AB and B–N based molecules such as the AB monomer and dimer, AB polymer, cyclotriborazane , and borazine inside narrow CNTs using DFT calculations. We found that all of these are energetically more stable inside the hollow (6, 6) CNT than in the vacuum. AB molecules favor the space inside a (6, 6) CNT, where they form an ordered chain, since they gain nearly 0.3 eV with respect to the crystalline environment. We distinguish two components of the energy gain that originate from either the intermolecular interaction or from the molecule-CNT interaction. Since the main purpose of introducing the CNT as a container is the narrow cylindrical cavity inside, we represented the CNT surrounding B–N based molecules by a soft potential well with cylindrical symmetry. The radial part of the potential well is determined by DFT calculations of the angularly and axially averaged interaction between the enclosed molecule and the graphitic nanotube wall. This approach correctly reproduces the interaction between B–N based molecules and the CNT wall, which – depending on the molecule – varies between −0.7 eV and −0.5 eV, while ignoring the discreteness of the carbon lattice. In absence of the AB-CNT interaction, AB molecules forming chains in this cylindrical potential are less stable by 0.21 eV than AB molecules in the molecular crystal. Taking the AB-CNT attraction into account, the AB molecule inside the CNT becomes more stable by 0.3 eV inside the CNT than in the crystal. Thus, AB molecules favor entering a narrow nanotube to form linear arrangements. The imposed geometry constraints may suppress formation of unwanted side products of the dehydrogenation reaction.

F. Rehydrogenation of PAB inside a carbon nanotube

As mentioned above, the most severe drawback in utilizing AB is the lack of any practical way to regenerate the initial AB system from its dehydrogenation products. As a working hypothesis, we assume that the reported benefits of enclosing AB in mesoporous media[20–23] are associated with constraining the degrees of freedom of AB and thus suppressing undesirable structural changes. Considering a narrow CNT as a generic enclosure for AB and its dehydrogenation products, we study in the following the rehydrogenation process of PAB in this environment and present our results in Fig. 3.

The calculated potential energy surface associated with the rehydrogenation process of PAB is shown in Fig. 3(a). We consider pairs of distances (d_{N-H}, d_{B-H}) within the unit cell as a useful way to determine a prejudice-free reaction coordinate, with the quantities defined in the inset of Fig. 3(b). Each point in the potential energy surface $E(d_{N-H}, d_{B-H})$, presented in Fig. 3(a), represents a structure that has been individually optimized by keeping only d_{N-H}, d_{B-H} and the unit cell size fixed. The schematic geometry of PAB inside a (6, 6) CNT, which is represented by the previously defined potential well in our calculations, is shown in Fig. 3(c). Since the potential energy surface in Fig. 3(a) is based only on structural optima, the dashed line connecting the open circles represents the energetically most favorable pathway from state E, corresponding to H_2 far away from PAB, across a potential energy barrier to state A, representing two AB molecules as the desired end-product of rehydrogenation. The corresponding energy profile along this pathway is depicted in Fig. 3(b) by the dashed line connecting the open circles. Snap shots of atomic arrangements and the charge density for selected intermediate structures are depicted in Fig. 3(d). Taking the system labeled M_1, representing the optimum structure of PAB and H_2 before hydrogenation, as a reference, the rehydrogenation step should require crossing an energy barrier of 3.5 eV. The abrupt energy change near the saddle point refers to an abrupt geometry change at that point, caused by a strong repulsion between PAB and H_2. We consider this an artifact and modify our optimization procedure by introducing the distance d_{B-N}, shown in the inset of Fig. 3(b), as an additional constraint to be optimized along the way in order to minimize the energy. This approach yields a rather smooth energy profile, represented by the solid line connecting the solid data points in Fig. 3(b). This smoother trajectory indicates that rehydrogenation of PAB, which involves simultaneous breaking of H_2 and B–N bonds while H–B and H–N bonds are forming, occurs with a lower energy

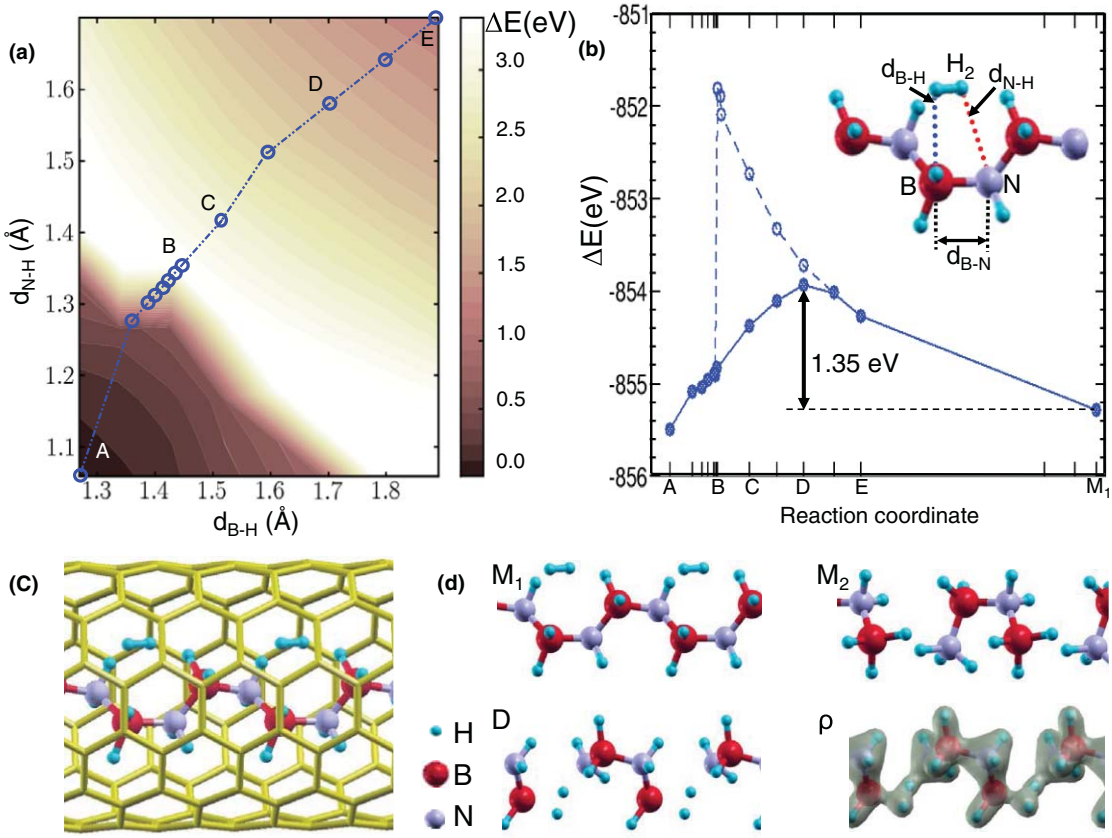

FIG. 3. Microscopic pathways of the rehydrogenation process. (a) Contour plot of the potential energy surface as a function of d_{B-H} and d_{N-H}, with the quantities d_{B-H} and d_{N-H} defined in the inset of (b). The dashed line is the optimal pathway of the rehydrogenation process. (b) Potential energy profiles along the reaction coordinate of the rehydrogenation processes. The dashed line and open circles are the exact energy profile along the reaction coordinate on the potential energy surface. The solid circles and the solid line are the energy profile obtained by placing an additional constraint on d_{B-N}. (c) The system considered in our rehydrogenation calculation, consisting of PAB and H_2 inside a (6, 6) CNT. (d) Snapshots of structures labeled M_1, M_2, D in (a)-(b), where M_1 is the globally relaxed geometry of state E and M_2 that of state A. ρ represents the $0.08\, e/a_0^3$ charge density isosurface of the geometry D.

barrier of 1.35 eV. In the intermediate structure D, depicted in Fig. 3(d) along with the associated charge density ρ, we can observe hybridization of orbitals associated with the hydrogen molecule and the B–N bond. From this state, H_2 dissociation and hydrogenation of the separated AB dimers, seen in the M_2 structure in Fig. 3(d), occur smoothly and complete the PAB rehydrogenation process.

IV. SUMMARY AND CONCLUSIONS

We have investigated atomistic mechanisms governing hydrogen release and uptake processes in AB within the framework of density functional theory. We found that the dihydrogen bond network plays a crucial role in stabilizing the NH_3BH_3 molecular crystal. In particular, we found that the transition from the orthorhombic to the tetragonal molecular crystal structure of AB occurs in the temperature range between 200 and 300 K, and that the formation of DADB occurs via an activated exothermic process. Conversion of the NH_3BH_3 molecular crystal to the energetically preferred polymeric NH_2BH_2 and molecular hydrogen is a thermally activated process that can be promoted by the presence of DADB. We calculated potential energy surfaces for this and the reverse reaction in order to elucidate favorable pathways for the inter-conversion between AB and PAB plus H_2. We proposed to enclose AB in narrow carbon nanotubes as a generic narrow cylindrical container to limit the formation of undesirable side-products, such as the cyclic compound borazine, which hinder subsequent rehydrogenation of the system. We also explored the effects of nanoconfinement on the possible rehydrogenation pathways of AB and suggest the use of photoexcitation as a means to achieve dehydrogenation of AB at low temperatures.

ACKNOWLEDGMENTS

This work has been funded by the National Science Foundation Cooperative Agreement No. EEC-0832785, titled "NSEC: Center for High-rate Nanomanufaturing." Computational resources have been provided by the Michigan State University High Performance Computing Center. E.K. acknowledges the use of the CNM high performance computing cluster, Carbon, supported by the (U.S.) Department of Energy (DOE), Office of Science, Office of Basic Energy Sciences, under Contract No. DE-AC02-06CH11357.

[1]L. Schlapbach and A. Züttel, Nature (London) **414**, 353 (2001).
[2]F. Mertens, G. Wolf, and F. Baitalow, in *Handbook of Hydrogen Storage: New Materials for Future Energy Storage*, edited by M. Hirscher (Wiley-VCH, Berlin, 2010), pp. 215–247.

[3]G. Wolf, J. Baumann, F. Baitalow, and F. P. Hoffmann, Thermochim. Acta **343**, 19 (2000).
[4]Freedom CAR/DOE hydrogen storage technical targets, see http://www.eere.energy.gov/hydrogenandfuelcells/pdfs/freedomcar_targets_explanations.pdf (2005).
[5]S. G. Shore and R. W. Parry, J. Am. Chem. Soc. **77**, 6084 (1955).
[6]F. Baitalow, J. Baumann, G. Wolf, K. Jaenicke-Rossler, and G. Leitner, Thermochim. Acta **391**, 159 (2002).
[7]J. Baumann, E. Baitalow, and G. Wolf, Thermochim. Acta **430**, 9 (2005).
[8]R. Schellenberg, J. Kriehme, and G. Wolf, Thermochim. Acta **457**, 103 (2007).
[9]C. R. Miranda and G. Ceder, J. Chem. Phys. **126**, 184703 (2007).
[10]M. E. Bluhm, M. G. Bradley, R. Butterick, U. Kusari, and L. G. Sneddon, J. Am. Chem. Soc. **128**, 7748 (2006).
[11]A. C. Stowe, W. J. Shaw, J. C. Linehan, B. Schmid, and T. Autrey, Phys. Chem. Chem. Phys. **9**, 1831 (2007).
[12]D. A. Dixon and M. Gutowski, J. Phys. Chem. A **109**, 5129 (2005).
[13]J. Li, S. M. Kathmann, G. K. Schenter, and M. Gutowski, J. Phys. Chem. C **111**, 3294 (2007).
[14]M. H. Matus, K. D. Anderson, D. M. Camaioni, S. T. Autrey, and D. A. Dixon, J. Phys. Chem. A **111**, 4411 (2007).
[15]V. S. Nguyen, M. H. Matus, D. J. Grant, M. T. Nguyen, and D. A. Dixon, J. Phys. Chem. A **111**, 8844 (2007).
[16]R. J. Keaton, J. M. Blacquiere, and R. T. Baker, J. Am. Chem. Soc. **129**, 1844 (2007).
[17]X. Z. Yang and M. B. Hall, J. Am. Chem. Soc. **130**, 1798 (2008).
[18]G. Soloveichik, J. H. Her, P. W. Stephens, Y. Gao, J. Rijssenbeek, M. Andrus, and J. C. Zhao, Inorg. Chem. **47**, 4290 (2008).
[19]Z. T. Xiong, C. K. Yong, G. T. Wu, P. Chen, W. Shaw, A. Karkamkar, T. Autrey, M. O. Jones, S. R. Johnson, P. P. Edwards, and W. I. F. David, Nature Mater. **7**, 138 (2008).
[20]A. Gutowska, L. Y. Li, Y. S. Shin, C. M. M. Wang, X. H. S. Li, J. C. Linehan, R. S. Smith, B. D. Kay, B. Schmid, W. Shaw, M. Gutowski, and T. Autrey, Angew. Chem., Int. Ed. **44**, 3578 (2005).
[21]A. Feaver, S. Sepehri, P. Shamberger, A. Stowe, T. Autrey, and G. Cao, J. Phys. Chem. B **111**, 7469 (2007).
[22]S. Sepehri, B. B. Garcia, and G. Cao, J. Mater. Chem. **18**, 4034 (2008).
[23]H. Kim, A. Karkamkar, T. Autrey, P. Chupas, and T. Proffen, J. Am. Chem. Soc. **131**, 13749 (2009).
[24]E. Artacho, E. Anglada, O. Dieguez, J. D. Gale, A. Garcia, J. Junquera, R. M. Martin, P. Ordejon, J. M. Pruneda, D. Sanchez-Portal, and J. M. Soler, J. Phys. Condens. Matter **20**, 064208 (2008).
[25]J. P. Perdew and A. Zunger, Phys. Rev. B **23**, 504f8 (1981).
[26]Density functional theory (DFT) calculations require a judicious choice of the exchange-correlation functional, since it is not *a priori* clear, whether the generalized gradient approximation (GGA), hybrid functionals, or the local density approximation (LDA) is most appropriate. In graphite, a well-documented example of a weakly interacting system, LDA reproduces correctly the equilibrium structure and elastic properties, whereas GGA fails in this respect. Van der Waals forces, which play an important role in such systems, are in reality not neglected in DFT, but enter in an approximate way through the exchange-correlation functional. Explicit treatment of van der Waals forces is desirable in systems, where these interactions dominate.
[27]N. Troullier and J. L. Martins, Phys. Rev. B **43**, 1993 (1991).
[28]L. Kleinman and D. M. Bylander, Phys. Rev. Lett. **48**, 1425 (1982).
[29]O. F. Sankey and D. J. Niklewski, Phys. Rev. B **40**, 3979 (1989).
[30]E. Artacho, D. Sánchez-Portal, P. Ordejón, A. García, and J. M. Soler, Phys. Status Solidi B **215**, 809 (1999).
[31]M. E. Bowden, G. J. Gainsford, and W. T. Robinson, Aust. J. Chem. **60**, 149 (2007).
[32]J. B. Yang, J. Lamsal, Q. Cai, W. J. James, and W. B. Yelon, Appl. Phys. Lett. **92**, 091916 (2008).
[33]D. J. Heldebrant, A. Karkamkar, N. J. Hess, M. Bowden, S. Rassat, F. Zheng, K. Rappe, and T. Autrey, Chem. Mater. **20**, 5332 (2008).
[34]W. T. Klooster, T. F. Koetzle, P. E. M. Siegbahn, T. B. Richardson, and R. H. Crabtree, J. Am. Chem. Soc. **121**, 6337 (1999).
[35]R. K. Raman, Z. Tao, T.-R. Han, and C.-Y. Ruan, Appl. Phys. Lett. **95**, 181108 (2009).